# Predicting cellular growth from gene expression signatures.

Edoardo M. Airoldi[1,2,†], Curtis Huttenhower[1,2,†], David Gresham[1,3], Charles Lu[1,3], Amy A. Caudy[1], Maitreya J. Dunham[4], James R. Broach[3], David Botstein[1,3,*], Olga G. Troyanskaya[1,2,*]

[1] Lewis-Sigler Institute for Integrative Genomics, Carl Icahn Laboratory, Princeton University, Princeton, NJ 08544

[2] Department of Computer Science, Princeton University, 35 Olden Street, Princeton, NJ 08540-5233

[3] Department of Molecular Biology, Princeton University, Washington Road, Princeton, NJ 08544-1014

[4] Department of Genome Sciences, University of Washington, 1705 NE Pacific Street, Seattle, WA 98195-5065

[†] These authors contributed equally to this work.

[*] To whom correspondence should be addressed. E-mail: ogt@genomics.princeton.edu, botstein@genomics.princeton.edu

**ABSTRACT.**

Maintaining balanced growth in a changing environment is a fundamental systems-level challenge for cellular physiology, particularly in microorganisms. While the complete set of regulatory and functional pathways supporting growth and cellular proliferation are not yet known, portions of them are well understood. In particular, cellular proliferation is governed by mechanisms that are highly conserved from unicellular to multicellular organisms, and the disruption of these processes in metazoans is a major factor in the development of cancer. In this paper, we develop a computational methodology to identify quantitative aspects of the regulatory mechanisms underlying cell proliferation in *Saccharomyces cerevisiae*. We find that the expression levels of a small set of genes accurately predict the instantaneous growth rate of any cellular culture, robust to changing biological conditions, experimental methods, and technological platforms. Our proposed model also predicts growth rates for the related yeast *Saccharomyces bayanus* and the highly diverged yeast *Schizosaccharomyces pombe*, suggesting that the underlying regulatory signature is conserved across a wide range of unicellular evolution. We investigate the biological significance of the identified gene expression signature from multiple perspectives: by perturbing the regulatory network through the Ras/PKA pathway, observing strong up-regulation of growth rate even in the absence of appropriate nutrients, and by discovering potential transcription factor binding sites enriched in growth-correlated genes. Our statistical model thus enables biological insights about growth at instantaneous time scales inaccessible by other experimental methods. Data and tools enabling others to apply this model are available at http://function.princeton.edu/growthrate.

**AUTHOR SUMMARY.**

A major challenge for living organisms is the regulation of cellular growth in a fluctuating environment. Sudden change in availability of nutrients or presence of stress factors typically requires rapid adjustments of cellular proliferation, and the misregulation of growth control in higher organisms is a major factor in the development of cancer. A statistical characterization of cellular growth based on gene expression levels thus provides a quantitative perspective to understand this regulatory network. We provide a model of cellular growth in the yeast *Saccharomyces cerevisiae* based on the expression levels of a small set of genes. Surprisingly, this model is able to predict the growth rate of new cultures from microarray expression data and is robust to changing biological conditions, experimental methods, and technological platforms. Such measurements of instantaneous growth rates at very short time scales are generally inaccessible by other experimental methods. The model also predicts growth rates in the related yeast *Saccharomyces bayanus* and in *Schizosaccharomyces pombe*, a yeast diverged by approximately a billion years of evolution. Our findings thus suggest that the model describes fundamental characteristics of the unicellular eukaryotic growth regulatory program. We use this information in a case study exploring the role of nutrient sensing in the yeast growth regulatory system.

## INTRODUCTION.

Proper regulation of growth rate is a key systems-level challenge for all cells, particularly microorganisms facing an ever-changing and often hostile environment. Cell growth, defined as an increase in cellular biomass due to biosynthetic processes, is one of the primary functions that must be coordinated with the environment in order for cells to maintain viability and reproduce. It is of central importance to our understanding of basic biology to determine how cells integrate information from the external environment and from their internal state to mount an appropriate response: growing in the presence of nutrients, arresting growth when stressed, and resuming afterwards. From a genomic perspective, growth also raises the issue of disentangling correlated systems-level behaviors and determining causality. When the expression levels of thousands of genes change due to a growth-related stimulus, which underlying regulatory parameters are responsible?

In this paper, we identify quantitative aspects of the transcriptional regulatory mechanisms underlying cell growth in *Saccharomyces cerevisiae* and develop a model to predict instantaneous growth rates of cellular cultures based on gene expression data. This provides a mechanism for estimating growth rates under any conditions for which microarray data is available, even at time scales too brief to measure with standard experimental techniques [1]. For example, a culture undergoing continuous growth in a chemostat [2] can be perturbed from steady state by means of a brief heat pulse, but the departure from and return to steady state growth is too brief to observe conveniently with optical density measurements. Our model allows such a decrease (and subsequent resumption) of growth rate to be quantified under a variety of conditions: batch or chemostat cultures, different microarray platforms, and under any environmental stimulus for which gene expression can be assayed. Surprisingly, this model also successfully predicts growth rates from *Saccharomyces bayanus* and *Schizosaccharomyces pombe* microarray data, the latter of which is evolutionarily diverged from *S. cerevisiae* by an estimated billion years [3].

This suggests that our statistical model of cellular growth can provide a broadly applicable biological characterization of the transcriptional regulatory network underlying growth rate control. We have previously observed that the expression of ~25% of the yeast genome responds to changes in growth rate [4]. This response is functionally cohesive, with genes upregulated with increasing growth enriched for translational and ribosomal functions and downregulated genes enriched for oxidative metabolism and the peroxisome. This provides a rich environment in which to study transcripitional growth regulation; for example, production of new proteins at the ribosome is vital to cellular proliferation, and yeast devotes some ~60% of its transcriptional throughput to ribosomal RNA [5]. Similarly, growth rate regulation is highly interconnected with a variety of other cellular processes (e.g. the environmental stress response [6], metabolic cycling [7], and the cell cycle [8]), and we discuss potential causative regulatory signals from the Ras/PKA pathway [9] and growth-related transcription factors.

Our recent analysis of gene expression measurements from a collection of *S. cerevisiae* chemostat cultures across several nutrient limitations and growth regimes [4] offered intriguing anecdotal evidence for an notion of effective growth rate. In this paper, we develop a model to characterize such a notion quantitatively, in a statistically principled fashion. We further assess the robustness of the proposed characterization by presenting new computational evidence on six additional published data sets and on four newly collected data sets. More in detail, we demonstrate that the model can accurately predict relative growth rates under a variety of conditions and is robust to the conditions of the originating culture, the technological platform used to assay gene expression, and evolutionary conservation to other organisms (*S. bayanus* and *S. pombe*). This allows us to predict growth rates for published microarray collections (e.g. the stress response [6] or gene deletions [10]) and for new data we have generated (Supplementary Tables S1-4), providing biological insight into the growth rate response at very short time scales—minutes, rather than the hours necessary to experimentally assay doubling times. These real-world biological predictions are accompanied by an out-of-sample validation and outlier analysis to establish the model's statistical

accuracy. We have made an implementation of this model available to the public at http://function.princeton.edu/growthrate.

In this paper, we also offer biological insights to that support and further substantiate the empirically observed robustness of the predictions based on the newly characterized growth-rate genes. Our insights rely on the quantitative identification binding motifs of known (and uncharacterized) transcription factors associated with the genes responding to growth, and on the quantitative characterization of growth profiles underlying puzzling experimental evidence that provides a first convincing explanation of observed cell death in response to a perturbation in the Ras/cAMP/PKA pathway. More in detail, we apply our model to specifically study two important aspects of cell growth regulation, nutrient sensing and the cell cycle. Artificial activation of the Ras/cAMP/PKA pathway has been previously observed to recapitulate approximately 85% of the expression response associated with increased growth in the presence of glucose [11]; here, we show that the cell's regulatory state during this activation is indicative of an upregulated growth response, even in the absence of appropriate nutrient availability. This conflict between internal regulatory state and the external environment leads to rapid cell death. In contrast, analysis of growth rate regulation during metabolic cycling [12] and synchronous cell cycles [8,13] indicates that growth rate regulation is not specific to cell cycle phases, but it is strongly limited to the oxidative phase of the metabolic cycle. These observations, coupled with an analysis of putative transcription factors mediating the growth response, establish a substantial foundation on which to base further experimental work on the systems-level control of cellular growth rate.

***Background: Measuring Growth***

Cellular growth is typically quantified in one of two experimental environments: batch culture or the chemostat. In a batch culture, cells are provided with a saturating amount of nutrient [1]. Growth is quantified by measuring the optical density (OD) of the cells over time. Figure 1 illustrates three phases of typical growth: a slow initial phase (lag), a fast exponential growth phase (exp), and a slow saturation phase (stationary). Solving the appropriate differential equation leads to an exponential model of cellular growth, $X = e^{\mu \cdot t}$. In practice, the OD of a culture is sampled at discrete points over time, and the growth rate parameter $\mu$ (in units of inverse hours $h^{-1}$) is estimated from an exponential fit to the OD measurements.

In the chemostat, a specific growth rate is maintained by limiting the concentration of a controlling nutrient provided to the cells [14]. Figure 2 illustrates the principle behind the chemostat. A limited concentration ($S_0$) of the controlling growth factor is provided in media flowing continuously into a growth tube of limited capacity. Changes in density of the culture (X) and in concentration of the controlling nutrient (S), in the growth tube, are driven by Michaelis-Menten dynamics [15]. In this regime, the growth rate is a function of the concentration of the controlling nutrient, $\mu = \mu(S)$. In particular, $dX/dt = [\mu(S) - D] X$; at steady state, the density of the culture no longer changes, $dX/dt=0$, and the concentration of the controlling growth factor also stabilizes, $dS/dt=0$. The growth rate then equals the flow rate set by the experimenter, $\mu(S^*)=D$.

In a batch culture, the growth rate is generally not controlled; it is determined by a complex interaction of environmental and genotypic states, and it is maximal during the exponential phase of growth ($\mu_{max}$). Under these conditions, the growth rate of the culture (the first derivative of the curve in Figure 1) changes with time. In a chemostat, the growth rate is controlled by setting the nutrient flow rate D below an organism's maximum possible growth rate $\mu_{max}$ as estimated from batch culture. In either experimental environment, the growth rate $\mu$ is directly related to the doubling time, $T_d = \ln(2)/\mu$.

Our model is built on a collection of gene expression data from chemostats at known growth rates, and it allows us to quantify a notion of instantaneous growth rate in chemostat and batch cultures, even in cultures in which the growth rate is changing rapidly over time.

## MATERIALS AND METHODS.

We fit a linear model to a collection of expression data drawn from *S. cerevisiae* chemostat cultures over several growth rates and nutrient limitations. This model provides estimates of parameters that characterize each gene's response to changes in growth rate, and these provide insight into the transcription factors and regulatory network responsible for yeast growth homeostasis. By applying this model to new expression data sets, we are able to predict instantaneous growth rates for any yeast culture. This inference process is robust to the biological and technical conditions of the originating gene expression data and predicts growth rates at instantaneous time scales inaccessible to standard experimental methods (e.g. optical density). We have also successfully applied the model to the related organisms *S. bayanus* and *S. pombe*. Data and tools relating to this model are made available at http://function.princeton.edu/growthrate.

### *Experimental Design and Data*

Our model is based on a collection of gene expression measurements from steady state (chemostat) cultures limited across several nutrients and growth regimes. Briefly, 36 CEN.PK derived *S. cerevisiae* chemostat cultures were grown under six nutrient limitations: Glucose (G), Nitrogen (N), Phosphate (P), Sulfur (S), Leucine (L), and Uracil (U). Six growth rates were used for each nutrient, ranging by steps of $0.05h^{-1}$ from $0.05h^{-1}$ to $0.3h^{-1}$. Agilent Yeast V2 microarrays were used to measure gene expression in the resulting 36 chemostats; for details, see [4]. This experimental design provides the opportunity to discover gene expression patterns correlating with growth rate independently of nutrient-specific responses.

Figure 3 highlights the sources of variability in the gene expression profiles that the experimental design aims at capturing. The resulting data contain a number of characteristic gene expression patterns, including genes with strong growth-specific transcriptional regulation and negligible nutrient-specific response (Figure 3A). Other genes include a growth-specific expression component but are also strongly up- or down-regulated under specific nutrient limitations (Figure 3B). Finally, Figure 3C displays expression profiles that show unsystematic or negligible responses under these conditions. The linear model described below summarizes the variability in the expression profiles of individual genes specifically due to changes in growth rate, which leads to a characterization of *growth-specific calibration genes* such as those shown in Figure 3A. This growth-specific signature enables predictions of the instantaneous growth rate of any cellular culture based on the relative expression values these growth-specific genes.

Table 1 summarizes the collections of expression data analyzed in this study. Six collections were previously published by others, one was published in our previous work [4], and four are new to this study: 1. chemostats limited for different nitrogen sources, 2. heat pulses inducing a temporary departure from steady state growth, 3. artificial activation of the Ras/PKA pathway, and 4. *S. bayanus* diauxic shift and heat shock time courses. All gene expression collections were pre-processed as in [16]. The gene expression microarray values for all genes in the growth-specific signature are provided in supplementary Tables S1–4, respectively.

### *Linear Models and Identification of Growth-Specific Signature*

We sought to identify a small set of genes providing a quantitative summary of cellular growth rate regulation. These 36 chemostat-derived microarrays provided us with the opportunity to determine which genes were responding consistently (i.e. linearly) and only to changes in growth rate (and not to differences in nutrient limitation). To model this statistically, we performed four steps, beginning by using maximum likelihood to fit a linear model of each gene $g$'s expression under all training conditions ($\mathbf{Y}_g$) based on the conditions' known growth rates ($\mathbf{X}_c$):

$$\mathbf{Y}_g = \alpha_g + \beta_g \mathbf{X}_c + \varepsilon_g \qquad (1)$$

This yields two learned parameters per gene, a baseline expression level $\alpha_g$ and a growth rate response $\beta_g$. The model is fit to minimize the residual error $\boldsymbol{\varepsilon}_g$, which can represent either non-growth-related biological variability or technical noise. We fit this model for the yeast genome using the expression levels from our 36 chemostat conditions, recording each gene's $\alpha_g$ and $\beta_g$ parameters and its goodness of fit (total explained variability) $R^2_g$.

We next used the bootstrap (i.e. a randomized re-sampling technique) to assess the expected background distributions of these parameters in the absence of a growth-related biological signal (i.e. the null distributions). We constructed 100,000 randomized expression vectors of length 36 by sampling each condition from all equivalent growth across all genes and nutrient limitations. For example, the first value randomly chosen for such a vector could be drawn from any gene or nutrient limitation in our chemostat data at a flow rate of $0.05h^{-1}$, the second from any flow rate of $0.1h^{-1}$, and so forth. Note that by re-sampling the expression values of putative genes column-by-column, we do not wash away the average transcriptional response that is expected to be associated with nutrient-growth rate pairs. In this sense, the null distribution we derive carries information about how genes respond to growth across nutrient limitations, on average. As a consequence, the statistical significance of the differential response we compute is biologically justified. In other words, this sampling scheme maintains average nutrient specific and growth rate specific information, and leads to an estimate of the null distribution in the absence of gene-specific growth related and nutrient related gene expression. This process yields null distributions for parameters $\alpha_g$, $\beta_g$, and the goodness of fit $R^2_g$.

Third, from these null distributions, we assign false discovery rate corrected p-values [17] to each gene's $\alpha_g$, $\beta_g$, and $R^2_g$ values. Finally, a gene was deemed to have a significant expression response to changes in growth rate if it fit this model well ($R^2_g$ $p<0.05$) and was up- or down-regulated significantly with growth ($\beta_g$ $p<0.05$); this information is available in [4]. We further characterized a specific set of *growth-specific calibration genes* responding only and significantly to changes in growth rate ($\beta_g$ $p<10^{-5}$ and $R^2_g$ $p<10^{-5}$) that we used to infer instantaneous growth rates in new expression data (Supplementary Table S5, Supplementary Data Archive S1).

***Model-Based Prediction of Instantaneous Growth Rates from Expression Data***

The set of growth-specific calibration genes defined above represents a quantitative signature of a cellular culture's transcriptional regulation of growth rate, i.e. the speed at which its cells are proliferating. By examining these genes' expression levels in new data, we can thus predict the instantaneous growth rate of the originating cellular culture. This instantaneous growth rate is comparable to the derivative of an optical density growth curve, but it can be inferred robustly by our model on any time scale (e.g. minutes) from microarray data without the need to measure one or more full doubling times of a culture.

Given expression data for a new experimental condition, we use an iterative maximum likelihood approach to infer its growth rate using the parameters captured by our linear model. Formally, consider a vector of expression measurements for $n$ calibration genes, $\mathbf{Z}_{1:n}$. As described above, the expression of these growth-specific genes varies primarily in response to changes in a condition's growth rate, which we model as the mean $\mu$ of a Gaussian with variance $\sigma^2$. Using our previously calculated maximum likelihood estimates of the calibration gene parameters $\boldsymbol{\alpha}_{1:n}$ and $\boldsymbol{\beta}_{1:n}$, the expected value of a gene's expression is thus:

$$\mathbb{E}[Z_i] = \alpha_i + \beta_i \mu + \delta \tag{2}$$

Here, $\delta$ is a condition-specific parameter capturing the condition's baseline gene expression, i.e. an average offset between a new experimental condition and our training data. In dual-channel data, this represents differences between a new condition's reference channel and our training data; for a single-channel array, it captures the absolute difference between the platform baseline and our training data. Similarly, the expected variability is:

$$\mathbb{V}[Z_i] = \beta_i^2 \sigma^2 \tag{3}$$

The likelihood of the expression measurements $\mathbf{Z}_{1:n}$ is thus a product of Gaussians:

$$\mathbb{L}\,(Z_{1:N}) = \prod_{i=1}^{n} \; Gaussian\,(\alpha_i + \beta_i \cdot \mu + \delta,\;\; \beta_i^2 \cdot \sigma^2). \tag{4}$$

From this, we derive the maximum likelihood estimate of the condition's growth rate $\mu_{ML}$:

$$\mu_{ML} = \frac{1}{n} \sum_{i=1}^{n} \frac{Z_i - \alpha_i - \delta_{ML}}{\beta_i} \tag{5}$$

Similarly, the maximum likelihood estimate of the condition's baseline $\delta_{ML}$ is given by:

$$\delta_{ML} = \frac{1}{n} \sum_{i=1}^{n} Z_i - \alpha_i - \beta_i \mu_{ML} \tag{6}$$

Note that the estimate of $\delta_{ML}$ depends on the estimate of $\mu_{ML}$, and vice versa. To calculate these estimates, we initialize $\mu_{ML}^{(0)}$ assuming $\delta_{ML}^{(0)}=0$ and iterate subsequent computations of $\mu_{ML}^{(t+1)}$ and $\delta_{ML}^{(t+1)}$ to convergence. In practice, growth-specific calibration genes with residuals outside the inner fences of all calibration gene residuals (more than 1.5 interquartile ranges from the lower or upper quartiles, [18]) are noted as outliers and removed from that condition's growth rate inference. This allows outlier genes responding to non-growth related stimuli (which are, in general, infrequent, e.g. six in one of our most variable conditions as discussed below) to be noted for further investigation while also decreasing the cross-validated error of predicted growth rates.

***Extending Predictions to Additional Organisms***

In principle, this model of growth rate can be extended to study and predict instantaneous growth in any organism for which appropriate homology exists to our set of growth-specific calibration genes. To analyze growth rates in expression data from *S. bayanus* and *S. pombe*, the *S. cerevisiae* calibration genes were mapped to known orthologs. This mapping was performed using the unambiguous pairings from [19] for *S. bayanus* and the curated orthologous groups from [20] for *S. pombe*. This resulted in 51 growth-specific genes for *S. bayanus* and 74 for *S. pombe*, the increase being due to one-to-many mappings; see Supplementary Table S5.

***Online Tool Availability***

The data driving our model (individual genes' growth rate response parameters) and tools allowing users to predict growth rates in new data sets are available at http://function.princeton.edu/growthrate. Specifically, users can upload *S. cerevisiae* expression data (single- or dual-channel in standard PCL format) to receive estimates of relative growth rate for each condition. If a reference with known growth rate is provided, absolute rate estimates will be generated. This growth rate prediction tool has been implemented in R and is also available for offline use, allowing further customization (such as application to additional organisms).

**RESULTS.**

We apply our linear model of growth rate regulation to predict instantaneous growth rates for a variety of expression data. This includes new chemostat cultures used to assess prediction quality, publicly available stress response and gene deletion microarrays from batch cultures, growth differences between metabolic cycling and the cell cycle, several different microarray platforms, and an out-of-sample validation to

quantify model accuracy. We also observe good predictive performance for growth rates in *S. bayanus* and *S. pombe* data sets, the latter despite up to a billion years of evolutionary divergence from our *S. cerevisiae* training data. This suggests that the growth-related transcriptional regulation captured by our model is a key feature of unicellular homeostasis, a feature we explore by examining nutrient sensing inputs through the Ras/PKA pathway and potential growth rate transcription factors and binding sites.

***Relative Growth Rate Prediction in Novel Experimental Settings***

Our model of the growth rate transcriptional response can be used to predict relative instantaneous growth rates from any *S. cerevisiae* gene expression data. For example, Figure 4A shows our predicted growth rates for a gene expression time course sampled from a steady state culture exposed to a brief (<30s) heat pulse (Supplementary Table S1). The predictions clearly show a departure from steady state within five minutes of the heat pulse, followed by recovery within 15 minutes. Similar predictions over a range of chemostat flow rates (Supplementary Figure S1) reveal that this cellular behavior is consistent, although there is some variation in the degree of growth cessation during stress, in agreement with tolerance and sensitization models of the yeast stress response [21]. Notably, standard experimental assays for growth rate (e.g. optical density) would be incapable of monitoring such a response, while our model is able to observe these growth changes on an instantaneous time scale.

A similar application of our model to predict relative growth rates for the stress response conditions of [6] is presented in Figure 4B (see Supplementary Figure S2 for complete results). These data represent batch yeast cultures assayed using a variety of different reference mRNA samples on a custom spotted microarray platform, none of which differences from our training data impair the growth rate estimation process. While there are no direct measurements of growth rate in these non-steady-state conditions, our predictions are consistent with known yeast biology and agree with expected growth behavior. Most shock time courses, including all heat shocks, peroxide, diamide, and hyper-osmotic stress, provoke an initial sharp decrease in growth rate followed by a return to initial or near-initial rate; shorter shocks, such as DTT, menadione, and peroxide responses, capture only the rate decrease. Batch growth proceeds at a fairly constant rate until nutrients become depleted, at which point the rate decreases sharply; this pattern is also seen in intentional nitrogen depletion. Growth rates across varying temperatures peak as expected at 25C [1], falling off at lower and higher temperatures. Finally, response to varying carbon sources is also as expected [22], with ethanol inducing the slowest growth and fructose, sucrose, and glucose allowing the most rapid. Our model's inference of growth rate from gene expression data alone thus allows both post hoc growth analysis (e.g. years after the original experiment) and an estimation of growth rates for cultures where it would be difficult or time consuming to measure directly.

When applied to microarray data from yeast mutants, in which one or more genes have been deleted, predicted growth rates can be used to approximate single mutant fitnesses. We used our model to analyze the knockout collection assayed in [10]; predictions on the complete data set are available in Supplementary Table S6. [10] provides direct fitness measurements for 199 of the ~300 mutants assayed by the microarrays. Our predictions for these 199 growth rates correlate very strongly with their measured values ($\rho=0.473$, $p<10^{-11}$) and are derived solely from expression data. In contrast, methods for experimentally estimating single mutant fitness from high throughput growth curves showed substantially less agreement ($\rho=0.321$, $p<10^{-6}$ [23]; $\rho=0.108$, $p>0.2$ [24]) with the original publication's direct measurements. This represents a compelling argument as to the relevance of our growth rate model for fitness estimation.

***Absolute Growth Rate Prediction with One Shared Reference***

With a small amount of additional information, the relative growth rates inferred by our model can be made absolute in units of chemostat flow rate ($hr^{-1}$). Our model's predicted rates are typically relative values; this is due to the unknown quantitative effects of the reference mRNA in our dual-channel training data. It is impossible to know a priori the relationship between this reference channel and the relative (for

dual-channel) or absolute (for single-channel) expression levels in new microarray data. However, if an absolute growth rate is known for some microarray condition in the data set, our model can make absolute rate predictions for other two-color data sharing the same reference channel.

Figure 4C shows actual growth rates (dotted, black lines) for a collection of chemostats at various flow rates limited on one of several different nitrogen sources (Supplementary Table S2) along with estimates of the relative instantaneous growth rates (red, dashed lines) and of the absolute instantaneous growth rates (solid, blue lines). Absolute growth rates are estimated by recording the growth rate in the Proline limited chemostat at $\mu=0.35hr^{-1}$, and shifting all the estimates accordingly, since the dual-channel microarrays in this study all share the same transcriptional readout in the reference channel. On normalized dual-channel microarrays, the doubling of any gene's mRNA level in these conditions results in a constant increase in its expression readout. This allows one unit of our predicted relative rates to correspond to one unit of absolute chemostat flow rate. However, since the reference channel differs from that of our training data, all rate predictions are vertically shifted by a corresponding constant factor. By normalizing to any one of the 24 conditions' known growth rates, this shift can be automatically corrected for the 23 other microarrays employing the same reference channel. We sought to evaluate the goodness of the predictions in Figure 4C by computing the statistical significance of their correlation with the actual growth rates. To this end, we computed the correlation between the true growth rates and the predicted instantaneous growth rates. The correlation is the same for both absolute and relative predicted rates, as they differ by a constant, and equals $\rho=0.956$ (p-value $\approx 0$). This computation provides statistical support to the goodness of the predictions produced with the proposed model.

***Accuracy of the Predictions and Outlier Detection***

We assessed the quality of our growth rate predictions using 1,000 out-of-sample experiments, according to a hybrid bootstrap/cross-validation setup, using the data from [4]. Results are shown in Figure 5A. In each experiment, we randomly withheld 12 of the 36 conditions for testing, fit our linear model on the remaining 24, derived bootstrapped null distributions using only these data, and determined calibration gene sets to use for growth rate inference on the held-out conditions. This experimental setup leads to absolute growth rate predictions directly, as all the dual-channel microarrays share the same transcriptional readout in the reference channel. This out-of-sample validation allowed us to assess the accuracy and variability of our predictions on conditions with known growth rates not included in the model building procedure. In addition to the performance indicated by Figure 5A, this demonstrated robustness to the stringency of p-value cutoffs and number of growth-specific calibration genes; these ranged in number from ~50 to ~110 across the randomized validations (of a total ~5,500 possible genes), and changes of this magnitude in the final calibration gene set had little impact on predicted growth rates. We further quantified a notion of reliability for each of the 72 growth-specific genes. Specifically, we computed the percentage of bootstrap experiments in which each individual gene was selected as a member of the growth-specific gene set. The percentages provide an expectation about whether each individual gene should be considered reliable in a new study. We found that 69 genes were selected in more than half of the experiments, $P > 0.5$. Full results are reported in Table 2.

In the process of estimating growth rates and determining this confidence score, growth-specific calibration genes with outlying expression values are also detected. While most conditions induce few outlying growth-specific genes, when they occur, they are *not* indicative of the quality of growth rate predictions. We have found that neither the number of outliers nor their variability correlates with prediction error (data not shown), but they call out genes that may be responding to non-growth stimuli under specific biological conditions. Excluding outliers from the growth rate estimation process improves the accuracy of the predictions, and these outliers can in turn be biologically informative: an outlying calibration gene is likely responding specifically to a stimulus other than change in growth rate. For example, some of the only outliers in the mild heat shock time course from [6] occur towards the end of a shift from 29C to 33C

(Figure 5B). These include *HSP26* and *HSP78*, both known heat shock chaperones [25,26]. Three genes of unknown function (*YLR327C*, *MOH1* and the neighboring dubious ORF *YBL048W*, and *TMA10*) are also outliers in this condition, which is evidence that these genes may have specific expression responses (and thus biological functions) during heat shock. *HSP26* and *YLR327C* are frequent outliers in stress-related conditions, perhaps suggesting a more general stress response function.

### *Predicting Growth Rates in* S. bayanus *and* S. pombe

While our growth rate model is based on a transcriptional growth signature in *S. cerevisiae*, the model can be applied to any organism with sufficiently orthologous transcriptional activity. This is likely to be the case within the *sensu stricto* yeasts, separated by ~25 million years of evolution [27]. By finding the ~50 *S. bayanus* genes orthologous to our ~70 *S. cerevisiae* growth-specific calibration genes [19], we can apply our model directly to *S. bayanus* expression data (Supplementary Table S4). Figure 6 demonstrates such a result for two *S. bayanus* time courses assaying the diauxic shift and a response to heat shock. These results have comparable profile to those from *S. cerevisiae* and are similarly biologically compelling. For example, the diauxic shift in *S. bayanus* results in a very similar growth pattern to the known response in *S. cerevisiae*, with a near-cessation of growth during the shift and subsequent rebound. Conversely, *S. bayanus* is less resistant to high temperatures than *S. cerevisiae* [28], and our growth rate inferences show a corresponding failure in its ability to grow following severe heat shock.

We have also extended our model to a significantly further diverged yeast, specifically the yeast *Schizosaccharomyces pombe*, separated from *S. cerevisiae* by an estimated one billion years of evolution [3]. A mapping of our growth-specific calibration genes to *S. pombe* using information from [20] results in ~75 genes due to one-to-many correspondences, but these provide sufficient calibration information to make high quality predictions (Figure 6C). Calibration gene outliers and expression cohesiveness are not substantially changed relative to *S. cerevisiae* and *S. bayanus*, and the inferred relative rates reflect various biological expectations. All cultures (data from [29]) show an initial increase from low growth rates due to stalled growth during synchronization. An expected decrease in growth rate is predicted during increased exposure to hydroxyurea (HU), and a *rad3*Δ deletion (*S. cerevisiae* ortholog *MEC1*) incurs a mild overall growth impairment as well as exacerbating HU sensitivity. While *MEC1* is essential in *S. cerevisiae*, this sensitivity has previously been noted for deletions *sod1*Δ and *lys7*Δ, both members of the MEC1 pathway [30], which is necessary for the cell cycle checkpoint function.

The extent to which transcriptional regulation is conserved between *S. cerevisiae* and *S. pombe*, which allows us to successfully apply the model despite the evolutionary distance that separates these species, is reflective of cellular growth's central role, particularly in unicellular organisms. While this model would become less meaningful in metazoans, where the growth of individual cells is subjugated to the growth and differentiation of the organism as a whole, certain transcriptional growth behavior is of necessity conserved in single celled organisms [31]. This is particularly true of the ribosome, one of the main contributors to our model's predictive power; rRNA regulation is purely transcriptional, and ribosomal proteins must be expressed stoichiometrically. Since any cellular growth requires translation, observation of ribosomal transcription is a strong indicator of unicellular growth [5]. This is one aspect of the transcriptional growth response made quantitative by our model.

### *Insights into Growth Homeostasis*

To further investigate the biological basis of growth rate correlated gene expression, we used our model to predict relative growth rates for two interesting cases: the yeast metabolic cycle [12] and the mitotic cell division cycle [8,13]. The microarray data published by Tu et al. was obtained for cells grown at high density in a glucose-limited chemostat. Under this regime, cells within the culture become metabolically synchronized and undergo periodic consumption of oxygen (defined as the oxidative phase of the metabolic cycle) followed by periods of undetectable oxygen consumption (termed the reductive building and

reductive charging phases). The cell cycle data sets by Spellman et al and Pramila et al were obtained from experiments in which cells were uniformly arrested in the cell division cycle using a variety of methods and then released to undergo synchronous cell division cycles.

Growth rate prediction applied to the yeast metabolic cycle data revealed a striking periodicity (Figure 7A). The cyclical pattern of growth rate variation occurs completely in concert with the metabolic cycle as defined by Tu et al. Specifically, the culture's growth rate is predicted to be at minima during the reductive phase of the metabolic cycle, when oxygen consumption is at a minimum, and reach maxima during the peak of the oxidative phases when oxygen consumption is maximal. In contrast, growth rate prediction for the cell cycle (Figures 7B and 7C) show virtually no variation in predicted growth rate during the different stages of cell division.

These data support and extend our previous assertions [4] that the there is a close connection between the metabolic cycle identified in [7] and [12] and the association we identify between growth rate and gene expression levels. This result is consistent with two possible explanations. The first is that there is variation in the growth rate of cells throughout the metabolic cycle. [12] and [32] have shown that under their specific experimental conditions, DNA replication and cell division is restricted to the reductive phases of the metabolic cycle. It is conceivable that growth per se (i.e. the accumulation of biomass) is paused during the reductive phases of the metabolic cycle so that the cell can replicate and segregate DNA and complete the complex processes of cell division; growth may then be restricted to the oxidative phase of the metabolic cycle. Alternatively, it is possible that as any heterogeneous culture grows faster, a greater fraction of cells are in the oxidative phase at any point in time. Thus, the growth rate gene expression signature we detect might reflect the fraction of cells in the oxidative and reductive phases of the metabolic cycle in a metabolically unsynchronized population.

The absence of growth rate differences during the cell division cycle (Figures 7B and 7C) supports our previous claim [4] that the growth rate expression signature is unrelated to the cell cycle. Moreover, since the published cell cycle experiments were performed in rich media using a fermentable carbon source, the results suggest that rapidly growing cells (which are almost exclusively fermenting) do not partition metabolic activity into discrete phases, as their energetic requirements are met in a continuously reductive metabolic state. It is only when slowed growth is imposed upon the cell, due to stress, nutrient limitation, or other suboptimal environments, that the metabolic cycle is required.

We sought to distinguish whether nutrient availability directly determines the transcriptional state related to growth rate or whether nutrient availability is integrated through an internal signaling pathway that controls the appropriate transcriptional state. To address this issue, we examined the regulatory circuit responsible for transcriptional changes in response to glucose availability in yeast. Glucose addition to cells growing on glycerol elicits a rapid and massive change in the pattern of gene expression, with more than half of all genes changing at least twofold in expression. Previous work has shown that the Ras/cAMP/PKA pathway is the major source for eliciting this transcriptional change in response to glucose addition [9,11]. Activation of the Ras/PKA pathway in the absence of environmental signals, through induction of an activated allele of *RAS2* ($RAS2^{G19V}$), recapitulates in magnitude and direction more than 85% of the changes observed by glucose addition, and inhibition of PKA (concurrent with addition of glucose) blocks most of the glucose induced transcriptional changes ([11], Supplementary Table S3). This mutation thereby represents a useful model connecting *S. cerevisiae*'s glucose sensory signaling to its transcriptional regulation of growth rate.

We used a *gal1*Δ strain carrying the activated allele $RAS2^{G19V}$ under control of the galactose inducible *GAL10* promoter. Addition of galactose activates the Ras/PKA pathway, but since galactose cannot be metabolized by this strain, the metabolic state of the cell remains unaltered [9]. When grown on glycerol our model predicts a relative growth rate of ~0.2 for this strain (Figure 8A), which changes to ~0.6 within twenty minutes following glucose addition, consistent with the change in doubling time from 5.8hr to

2.6hr. When we performed the same experiment on glycerol media and induced the *RAS2*$^{G19V}$ by means of galactose addition, we detected a transcriptional response within sixty minutes. The predicted growth rate of the *RAS2*$^{G19V}$ mutant strain was comparable to the addition of glucose despite the fact that galactose addition does not yield an increase in growth, as measured by optical density, since the cells are unable to metabolize galactose. In fact, while the model's summarization of gene expression state indicates that the culture is attempting to increase growth, induction of the *RAS2*$^{G19V}$ allele results in an immediate decrease in growth rate and complete cessation of growth within four hours [33]. These results are consistent with the cell setting its growth-specific transcription program on the basis of its *perception* of nutrients present in the environment, rather than on the direct availability of energy or metabolites produced from such nutrients. The mechanism by which the cell integrates this external state in order to set the appropriate growth rate expression state must be mediated, at least in part, through the Ras/cAMP/PKA pathway.

***Potential Transcriptional Regulators of Growth Rate***

To investigate the regulatory basis of growth-associated gene expression, we identified motifs enriched in the 3' and 5' regions of genes with strong growth rate responses (Figure 8B). We assigned genes to clusters based on their growth rate response parameter ($\beta_g$) using k-means clustering with k=10. Using the FIRE motif identification program [34], we identified enriched motifs in seven of the resulting ten clusters. Consistent with the functional enrichments of negatively growth rate correlated genes [4], we identified known binding sites associated with the stress responsive transcription factors Msn2p and Msn4p in genes negatively correlated with growth rate. Conversely, genes that increase in expression with increased growth rate are enriched for the Rap1p consensus motif, which is commonly found upstream of genes encoding protein components of the ribosome.

We also found enrichment of the Ino4p binding site in genes upregulated with increasing growth rate. Ino4p forms a heterodimer with Ino2p to activate genes involved in phospholipid, fatty acid, and sterol biogenesis, all of which are required in greater abundance with increased growth rates. Furthermore, Ino4p has been proposed to have an inhibitory effect on a number of genes, including those that encode the heat shock proteins (Hsp12p, Hsp26p) and catalase (Ctt1p) [35]. We also identified two additional enriched motifs in the 5' UTR for which the binding factor is not known, suggesting that additional activators of growth-related transcriptional programs remain to be determined.

In addition to 5' upstream motifs, we identified five enriched 3'UTR motifs, which are potential binding site for proteins that promote mRNA degradation. Only a small number of mRNA binding consensus sequences are known in yeast, all of which belong to the Puf family of mRNA binding proteins [36]. Our analysis identified five enriched motifs in 3'UTRs. Two of these motifs, found in genes positively correlated with growth rate, were identified by the FIRE program as being targets of Puf4p. As an independent test, we compared the distribution of growth rate responses in the known gene targets of the five Puf proteins with the overall distribution of growth rate slopes. Targets of both Puf3p (220 genes) and Puf4p (205 genes) are enriched for genes that are upregulated with increasing growth (Wilcoxon-Mann-Whitney two sample p-values $9\text{x}10^{-23}$ and $7.23\text{x}10^{-16}$, respectively; Supplementary Figure S3). The consensus motifs of Puf3p and Puf4p are very similar; investigation of the PUF4 motif identified by FIRE suggests that the enrichment signal for at least one of the motifs denoted PUF4 is likely to result from a composite of Puf3p and Puf4p target genes (Figure 8B).

Overall, this analysis is consistent with tight transcriptional regulation underlying the cellular growth program; it is likely that mRNAs involved in this process are also subject to extensive post-transcriptional control. Interestingly, since our growth-rate prediction method is sensitive to changes in gene expression levels that occur within minutes of a perturbation, we expect that post-transcriptional regulation (both mediated decay of and stabilization of transcripts) is involved in this response. Experimental analyses of

the effects of perturbations within this regulatory network promise to shed further light on its organization.

**DISCUSSION.**

We present a statistical model of the gene expression response to changes in growth rate in *S. cerevisiae*. Based on microarray data from a variety of steady state growth rates and nutrient limitations, this model captures descriptive information regarding each gene's consistency and degree of response to growth rate. As detailed in [4], approximately half of the genome shows a significant transcriptional response to growth rate with strong functional cohesiveness; here, we extend this model to show its robustness, applicability to new data, and ability to provide insight into the biological systems driving cellular regulation of growth rate. New experiments with more complex models (quadratic and hierarchical) demonstrated that additional model parameters did not provide substantial performance gains, particularly relative to their added complexity (data not shown). Similarly, changes in the stringency of definitions of responding genes or of growth-specific genes did not substantially alter results. This is reflected in the out-of-sample validation results, which quantify the model's accuracy in predicting relative growth rates from gene expression data.

This model can be applied to new gene expression data to infer the relative instantaneous growth rate of the originating cellular culture. This instantaneous rate represents a measurement of the transcriptional state of cellular growth rate control, and it provides insight into the cell's growth rate at arbitrarily short time scales inaccessible by experimental measurements (e.g. optical density). Moreover, genes with outlying expression values can be detected during growth rate inference, calling out probable biological responses to specific non-growth stimuli. The predictions based on this model are robust to changing biological conditions, experimental methods, and technological platforms; they also scale from our *S. cerevisiae* training data to the related yeast *S. bayanus* and the highly diverged yeast *S. pombe*, suggesting that the transcriptional control of growth rate captured by the model are a fundamental aspect of unicellular biology.

Through further analysis of this regulatory network, we discovered several potential transcription factor binding sites enriched in growth-correlated genes, most notably the stress-responsive Msn2p and Msn4p, the Rap1p ribosomal factor, and Ino4p. Importantly, we have identified a likely role for post-transcriptional regulation in modulating transcriptional states related to growth rates. This finding is consistent with our ability to measure changes in growth rate over very short time scales using gene expression signatures. The abundance of any messenger RNA is a function of both its rate of production and of its rate of degradation; however, since transcription can be relatively slow, changes in abundance can be most rapidly effected by altering the stability of the extant mRNA population. The Puf proteins have known roles in mediating mRNA degradation [37] and in mediating the association of functionally related transcripts [36]. It has recently been proposed that modulation of mRNA stability is an important factor in metabolic regulation [38]. The association of Puf protein binding domains in the 3' UTRs of genes with increased expression at higher growth rates suggests that modulating mRNA stability is also important in the regulation of the growth response at short time scales.

From a computational perspective, it is notable that a simple linear model accurately and robustly captures a specific biological phenomenon. The model represents a concise, functionally cohesive set of expression profiles regarding the genome's transcriptional response to growth. This description agrees with known aspects of the growth response, such as the transcription of ribosomal components, and provides initial data as to the mechanistic roles of internal feedback, environmental sensing, and the stress response as growth rate varies. By monitoring an ensemble of genes - but with few parameters per individual gene - the model is easily applicable to new conditions and organisms and is robust to technical and biological variability. These features enable our model to serve both as a practical tool for growth rate estimation

(available at http://function.princeton.edu/growthrate) and as a mechanistic building block in the pursuit of a systems-level understanding of cellular growth processes.

**REFERENCES.**


1. Amberg DC, Burke DJ, Strathern JN (2005) Methods in yeast genetics: A Cold Spring Harbor Laboratory course manual: Cold Spring Harbor Laboratory Press.
2. Hayes A, Zhang N, Wu J, Butler PR, Hauser NC, et al. (2002) Hybridization array technology coupled with chemostat culture: Tools to interrogate gene expression in Saccharomyces cerevisiae. Methods 26: 281-290.
3. Hedges SB (2002) The origin and evolution of model organisms. Nat Rev Genet 3: 838-849.
4. Brauer MJ, Huttenhower C, Airoldi EM, Rosenstein R, Matese JC, et al. (2008) Coordination of growth rate, cell cycle, stress response, and metabolic activity in yeast. Mol Biol Cell 19: 352-367.
5. Warner JR (1999) The economics of ribosome biosynthesis in yeast. Trends Biochem Sci 24: 437-440.
6. Gasch AP, Spellman PT, Kao CM, Carmel-Harel O, Eisen MB, et al. (2000) Genomic expression programs in the response of yeast cells to environmental changes. Mol Biol Cell 11: 4241-4257.
7. Klevecz RR, Bolen J, Forrest G, Murray DB (2004) A genomewide oscillation in transcription gates DNA replication and cell cycle. Proc Natl Acad Sci U S A 101: 1200-1205.
8. Pramila T, Wu W, Miles S, Noble WS, Breeden LL (2006) The Forkhead transcription factor Hcm1 regulates chromosome segregation genes and fills the S-phase gap in the transcriptional circuitry of the cell cycle. Genes Dev 20: 2266-2278.
9. Wang Y, Pierce M, Schneper L, Guldal CG, Zhang X, et al. (2004) Ras and Gpa2 mediate one branch of a redundant glucose signaling pathway in yeast. PLoS Biol 2: E128.
10. Hughes TR, Marton MJ, Jones AR, Roberts CJ, Stoughton R, et al. (2000) Functional discovery via a compendium of expression profiles. Cell 102: 109-126.
11. Zaman S, Lippman SI, Zhao X, Broach JR (2008) How Saccharomyces Responds to Nutrients. Annu Rev Genet.
12. Tu BP, Kudlicki A, Rowicka M, McKnight SL (2005) Logic of the yeast metabolic cycle: temporal compartmentalization of cellular processes. Science 310: 1152-1158.
13. Spellman PT, Sherlock G, Zhang MQ, Iyer VR, Anders K, et al. (1998) Comprehensive identification of cell cycle-regulated genes of the yeast Saccharomyces cerevisiae by microarray hybridization. Mol Biol Cell 9: 3273-3297.
14. Novick A, Szilard L (1950) Description of the chemostat. Science 112: 715-716.
15. Monod J (1950) La technique de culture continue, theorie et applications. Ann Inst Pasteur 79: 390-410.
16. Huttenhower C, Hibbs M, Myers C, Troyanskaya OG (2006) A scalable method for integration and functional analysis of multiple microarray datasets. Bioinformatics 22: 2890-2897.
17. Benjamini Y, Hochberg Y (1995) Controlling the false discovery rate: a practical and powerful approach to multiple testing. J R Stat Soc Ser B 57: 289-300.
18. Moore DS, McGabe GP (2005) Introduction to the Practice of Statistics. New York: W. H. Freeman.
19. Kellis M, Patterson N, Endrizzi M, Birren B, Lander ES (2003) Sequencing and comparison of yeast species to identify genes and regulatory elements. Nature 423: 241-254.
20. Penkett CJ, Morris JA, Wood V, Bahler J (2006) YOGY: a web-based, integrated database to retrieve protein orthologs and associated Gene Ontology terms. Nucleic Acids Res 34: W330-334.
21. Attfield PV (1997) Stress tolerance: the key to effective strains of industrial baker's yeast. Nat Biotechnol 15: 1351-1357.
22. Granot D, Snyder M (1993) Carbon source induces growth of stationary phase yeast cells, independent of carbon source metabolism. Yeast 9: 465-479.
23. Warringer J, Blomberg A (2003) Automated screening in environmental arrays allows analysis of quantitative phenotypic profiles in Saccharomyces cerevisiae. Yeast 20: 53-67.

24. Jasnos L, Korona R (2007) Epistatic buffering of fitness loss in yeast double deletion strains. Nat Genet 39: 550-554.
25. Ferreira RM, de Andrade LR, Dutra MB, de Souza MF, Flosi Paschoalin VM, et al. (2006) Purification and characterization of the chaperone-like Hsp26 from Saccharomyces cerevisiae. Protein Expr Purif 47: 384-392.
26. Leonhardt SA, Fearson K, Danese PN, Mason TL (1993) HSP78 encodes a yeast mitochondrial heat shock protein in the Clp family of ATP-dependent proteases. Mol Cell Biol 13: 6304-6313.
27. Gao LZ, Innan H (2004) Very low gene duplication rate in the yeast genome. Science 306: 1367-1370.
28. Kishimoto M, Goto S (1995) Growth temperatures and electrophoretic karyotyping as tools for practical discrimination of Saccharomyces bayanus and Saccharomyces cerevisiae. Journal of General and Applied Microbiology 41: 239-247.
29. Chu Z, Li J, Eshaghi M, Peng X, Karuturi RK, et al. (2007) Modulation of cell cycle-specific gene expressions at the onset of S phase arrest contributes to the robust DNA replication checkpoint response in fission yeast. Mol Biol Cell 18: 1756-1767.
30. Carter CD, Kitchen LE, Au WC, Babic CM, Basrai MA (2005) Loss of SOD1 and LYS7 sensitizes Saccharomyces cerevisiae to hydroxyurea and DNA damage agents and downregulates MEC1 pathway effectors. Mol Cell Biol 25: 10273-10285.
31. Rudra D, Warner JR (2004) What better measure than ribosome synthesis? Genes Dev 18: 2431-2436.
32. Chen Z, Odstrcil EA, Tu BP, McKnight SL (2007) Restriction of DNA replication to the reductive phase of the metabolic cycle protects genome integrity. Science 316: 1916-1919.
33. Fedor-Chaiken M, Deschenes RJ, Broach JR (1990) SRV2, a gene required for RAS activation of adenylate cyclase in yeast. Cell 61: 329-340.
34. Elemento O, Slonim N, Tavazoie S (2007) A universal framework for regulatory element discovery across all genomes and data types. Mol Cell 28: 337-350.
35. Santiago TC, Mamoun CB (2003) Genome expression analysis in yeast reveals novel transcriptional regulation by inositol and choline and new regulatory functions for Opi1p, Ino2p, and Ino4p. J Biol Chem 278: 38723-38730.
36. Gerber AP, Herschlag D, Brown PO (2004) Extensive association of functionally and cytotopically related mRNAs with Puf family RNA-binding proteins in yeast. PLoS Biol 2: E79.
37. Olivas W, Parker R (2000) The Puf3 protein is a transcript-specific regulator of mRNA degradation in yeast. Embo J 19: 6602-6611.
38. Palumbo MC, Farina L, De Santis A, Giuliani A, Colosimo A, et al. (2008) Collective behavior in gene regulation: post-transcriptional regulation and the temporal compartmentalization of cellular cycles. Febs J 275: 2364-2371.

**TABLES.**

Table 1: Overview of expression data analyzed in this study. Of the 11 gene expression data sets for which we predict and discuss growth rates, four are previously unpublished; excerpts of this data relevant to the growth rate analysis are provided in supplementary Tables S1-4. These data span various experimental conditions, dual- and single-channel expression array platforms, batch and steady-state growth regimes, and three species of yeast. Under these varied conditions, our growth model predicts instantaneous growth rates and provides insight into regulatory mechanisms for growth homeostasis.

| Experimental conditions | Method | Platform | Organism | Publication/Experimenter |
|---|---|---|---|---|
| Nutrient-limited growth | Chemostat | Agilent | *S. cerevisiae* | [4] |
| Cell cycle synchronization | Batch | Spotted | *S. cerevisiae* | [13] |
| Cell cycle synchronization | Batch | Spotted | *S. cerevisiae* | [8] |
| Metabolic cycling | Batch/Chem. | Affymetrix | *S. cerevisiae* | [12] |
| Environmental stress | Batch | Spotted | *S. cerevisiae* | [6] |
| Gene deletion mutants | Batch | Spotted | *S. cerevisiae* | [10] |
| Heat pulses | Chemostat | Agilent | *S. cerevisiae* | C. Lu, Supplementary Table S1 |
| Nitrogen-limited growth | Chemostat | Agilent | *S. cerevisiae* | D. Gresham, Supplementary Table S2 |
| RAS/PKA activation | Batch | Agilent | *S. cerevisiae* | J. R. Broach, Supplementary Table S3 |
| Diauxic shift, heat shock | Batch | Spotted | *S. bayanus* | A. A. Caudy, M. J. Dunham, Supplementary Table S4 |
| Hydroxyurea response | Batch | Spotted | *S. pombe* | [29] |

Table 2: Reliability study for the 72 growth-specific genes. Reliability for an individual gene was quantified by computing the percentage of 1,000 bootstrap experiments where the gene was selected in the set of growth-specific genes. Results suggest that 69 genes are expected to be reliable in a new study, $P > 0.5$.

| Gene | Percentage | Gene | Percentage | Gene | Percentage | Gene | Percentage |
|---|---|---|---|---|---|---|---|
| UTR2 | 1 | NOP1 | 0.78 | HSP26 | 0.98 | HSP30 | 0.83 |
| AMS1 | 0.96 | OLI1 | 1 | DCS2 | 0.97 | GND2 | 0.87 |
| CTP1 | 0.64 | SNO4 | 0.97 | GSC2 | 0.84 | RPL24A | 0.62 |
| YOL014W | 1 | RPL7A | 0.97 | FUR1 | 0.57 | OM45 | 0.77 |
| HXT5 | 1 | HSP78 | 0.67 | MOH1 | 1 | BTN2 | 0.63 |
| YPT53 | 0.99 | RPL18A | 0.89 | RPL20A | 0.67 | POT1 | 0.74 |
| YJR008W | 0.61 | NCA3 | 1 | YHR138C | 0.6 | RPL31B | 0.69 |
| HSP32 | 0.96 | HSP42 | 1 | RPP2A | 0.89 | NDE2 | 0.75 |
| GPG1 | 1 | MSC1 | 1 | YLR312C | 1 | UGX2 | 0.63 |
| YBL048W | 1 | YDR379C-A | 0.57 | UIP4 | 0.96 | YDR070C | 0.8 |
| DDR2 | 0.99 | PAI3 | 0.95 | YGR043C | 0.97 | PHM7 | 0.76 |

| | | | | | | | |
|---|---|---|---|---|---|---|---|
| YJL161W | 0.94 | TFS1 | 0.79 | YLL067C | 0.63 | CTT1 | 0.7 |
| RPL23A | 0.65 | RPP1A | 0.89 | YMR196W | 0.93 | HSP12 | 0.62 |
| YOR338W | 0.62 | ROM1 | 0.56 | SPG1 | 0.84 | GPH1 | 0.63 |
| RPL18B | 0.82 | RPP1B | 0.81 | PET10 | 0.8 | SOL4 | 0.68 |
| SSE2 | 0.97 | SNU13 | 0.64 | RPS28A | 0.79 | YIR016W | 0.37 |
| HSP104 | 0.97 | YBR116C | 1 | YLR327C | 0.86 | GRE1 | 0.44 |
| AAC3 | 0.69 | IMD4 | 0.96 | YTP1 | 0.58 | GDH2 | 0.28 |

**FIGURE LEGENDS.**

Figure 1: *Growth phases of a typical cellular culture.*

Figure 2: *Schematic of a chemostat [14].*

Figure 3: *Representative genes responding to growth rate, specific nutrients, or unsystematically in our chemostat-derived training data.* Our statistical model of growth rate regulation is based on microarray data collected from 36 chemostats at six growth rates ($0.05hr^{-1}$ through $0.3hr^{-1}$) under six nutrient limitations (Glucose, Nitrogen, Phosphate, Sulfur, Leucine, and Uracil) as described in [4]. By employing the genes responding strongly, consistently, and only to changes in growth rate (and not specific nutrients) as growth-specific genes, we can apply our model to predict relative growth rates in new expression data. Gene expression in our original 36 conditions fell into three main categories as shown here. A) Genes strongly up- or down-regulated in response to changes in growth rate, independent of limiting nutrient. The most statistically significant members of this set became our growth-specific calibration genes for application of the linear model to other expression data. B) A subset of conditions highlighting genes with expression levels showing some correlation with growth rate, but with a strong nutrient-specific component. This represents a sizeable portion of the genome (~25%), with positively growth-correlated genes enriched mainly for ribosomal function and negatively correlated genes enriched for oxidative metabolism. C) A subset of conditions highlighting genes showing a non-systematic or negligible change in gene expression. Unresponsive genes were enriched for a variety of cellular processes not expected to show a strong relationship with growth, e.g. transcription, DNA metabolism and packaging, secretion, and many others.

Figure 4: *Predicted growth rates for S. cerevisiae gene expression data sets.* Our model of the growth rate transcriptional response can be used to predict the growth rate of a cellular culture from gene expression data, robust to the originating biological conditions, growth regime, and experimental platform. Here, we apply the model to three selected data sets to infer relative and absolute growth rates. A) A brief (<30s) heat pulse was administered to a steady state chemostat culture immediately before time zero, and gene expression was assayed with a microarray time course (see Supplementary Figure S1 and Supplementary Table S1). The relative growth rates inferred from this data show an abrupt departure from steady state growth, followed by a return to steady state (including a brief regulatory overshoot). Our predictions monitor these changes in growth rate at an instantaneous time scale (<5m) inaccessible by standard experimental assays for growth rate. B) Predicted growth rates for a portion of the [6] environmental stress response data, assaying the response to a 30–37°C heat shock. Our model captures the cessation and resumption of growth induced by the stress, even for a batch culture in which the growth rate is not fixed a priori. C) A collection of 24 chemostats were run at four growth rates ($0.05hr^{-1}$ through $0.2hr^{-1}$) and limited on six different nitrogen sources. Using only expression data from each condition, our model predicts accurate relative growth rates. However, when provided with the known growth rate for a single condition, the model is additionally able to infer absolute growth rates for all other data sets sharing that condition's mRNA reference channel. Note that the actual growth rate is measured empirically and thus deviates slightly from an ideal straight line due to technical variation in the growth equipment.

Figure 5: *Assessment of accuracy and outlier detection during growth rate inference.* A) We performed an out-of-sample cross-validation of our model by randomly sub-sampling 24 of the 36 training microarray conditions 1,000 times. We refit our linear model in each random sample, calculated bootstrapped null distributions for all gene parameters, and found sets of the most significant growth-specific genes. These were then used to infer growth rates for the 12 held-out conditions, providing an estimate of the accuracy of the model's growth rate predictions. B) When predicting the growth rate of a new collection of expression data, our model excludes any calibration gene with an expression level outside the inner fence (1.5 times the inter-quartile range below or above the first or third quartiles). This improves predicted growth rate accuracy while also calling out genes potentially responding to specific non-growth stimuli under some biological condition. For example, in the [6] mild heat shock time course, two of the six outliers are known heat shock genes (HSP26 and HSP78). The other four (YLR327C, MOH1, YBL048W, and TMA10) are uncharacterized genes, suggesting potential roles in the response to heat shock.

Figure 6: *Predicted growth rates for S. bayanus and S. pombe expression data sets.* By examining genes orthologous to our ~70 S. cerevisiae growth-specific calibration genes, we successfully applied our model to predict growth rates in S. bayanus (~50 orthologous growth-specific genes, ~20M years diverged) and S. pombe (~75 growth-specific genes due to one-to-many mappings, ~1B years diverged). A) Predicted growth rates for S. bayanus undergoing the diauxic shift from fermentative to respiratory growth (Supplementary Table S3). As observed for the S. cerevisiae diauxic shift in [4], growth pauses as glucose is exhausted and resumes as the yeast begins consuming ethanol. B) Predicted growth rates for S. bayanus exposed to a 25-37C heat shock (Supplementary Table S3). In contrast to Figure 4B, in which S. cerevisiae is observed to recover from a 37C heat shock, the less-thermotolerant S. bayanus (Kishimoto and Goto 1995) is predicted to halt growth at high temperatures. C) Predicted growth rates for S. pombe wild-type and rad3Δ time courses, grown normally and exposed to hydroxyurea (HU, an inhibitor of DNA synthesis and thus growth) (Chu et al. 2007). Despite the wide evolutionary divergence between S. pombe and our S. cerevisiae training data, predicted growth rates are in substantial agreement with expected biology. Each time course begins with low growth in a synchronized culture. When the synchronization block is released, cells begin growing, wild-type more efficiently than the rad3Δ mutant. Exposure to HU decreases growth over time, and this effect is exacerbated by RAD3 deletion. While the S. cerevisiae RAD3 ortholog MEC1 is essential, knockouts of the MEC1 pathway members SOD1 and LYS7 have been previously observed to induce HU sensitivity [30].

Figure 7: *Differences in growth characteristics of a metabolically cycling culture compared to cells synchronously undergoing the cell division cycle.* We predict periodic bursts of growth during the oxidative phase of the metabolic cycle as described by [12]. Conversely, we observe essentially no variation in growth in cultures synchronously undergoing the cell division cycle, which has been shown to primarily occupy the reductive phase of the metabolic cycle [32]. A) In cells undergoing metabolic cycling, growth rates are predicted to peak during the oxidative phase of the cycle, where [12] also observes strong upregulation of translational and ribosomal genes. B) The predicted growth rate for the [13] alpha-factor synchronized cell cycle is essentially constant, after an initial release from the synchronization block. C) Predicted rates for the [8] alpha-factor synchronized cell cycle also show an initial resumption of growth after alpha-factor block followed by relatively constant growth rate. Taken together, these observations support the claim that growth rate regulation is not specific to any one cell cycle phase. This also agrees with the fact that rapidly growing (and thus fermenting) S. cerevisiae does not partition metabolism into discrete stages, a phenomenon only occurring when reductive metabolism is hindered by nutrient limitation or other stresses.

Figure 8: *Perturbations and potential transcriptional regulators of the growth rate response.* A) Predicted growth rates for gal1Δ cells shifted to glucose, to galactose, and to galactose with a constitutively active RAS2G19V allele. On glucose, rapid growth is induced within ~40m; growth on galactose falls to low levels within ~40m, as it cannot be metabolized by this mutant. However, when glucose sensing is emu-

lated by artificial activation of the Ras/PKA pathway, the transcriptional regulatory network attempts to induce rapid growth within ~60-80m despite the unavailability of appropriate nutrients. This disconnect between actual and perceived cellular state leads to cell death within 4-6 hours and suggests that nutrient sensing (as opposed to metabolic activity or internal cellular state) is responsible for a large portion of the transcriptional growth rate response. B) Regulatory binding sites enriched in growth up- and down-regulated genes. We clustered the yeast genome by degree of growth rate response, yielding ten clusters with average responses ranging from -12.0 (strongly downregulated with increasing growth rate) to 8.6 (strongly upregulated). The FIRE program [34] predicted 10 regulatory motifs in the upstream flanks and 3' UTRs of the most up- and down-regulated clusters. These included the known stress-responsive MSN2/4 binding sites in downregulated genes, the ribosomal regulators RAP1 and PUF4 in upregulated genes, and INO4 sites in upregulated genes (possibly corresponding to its role in the stress response and fatty acid biosynthesis [35]. We also identified five additional putative growth regulatory sites for which the binding factor is not yet known.

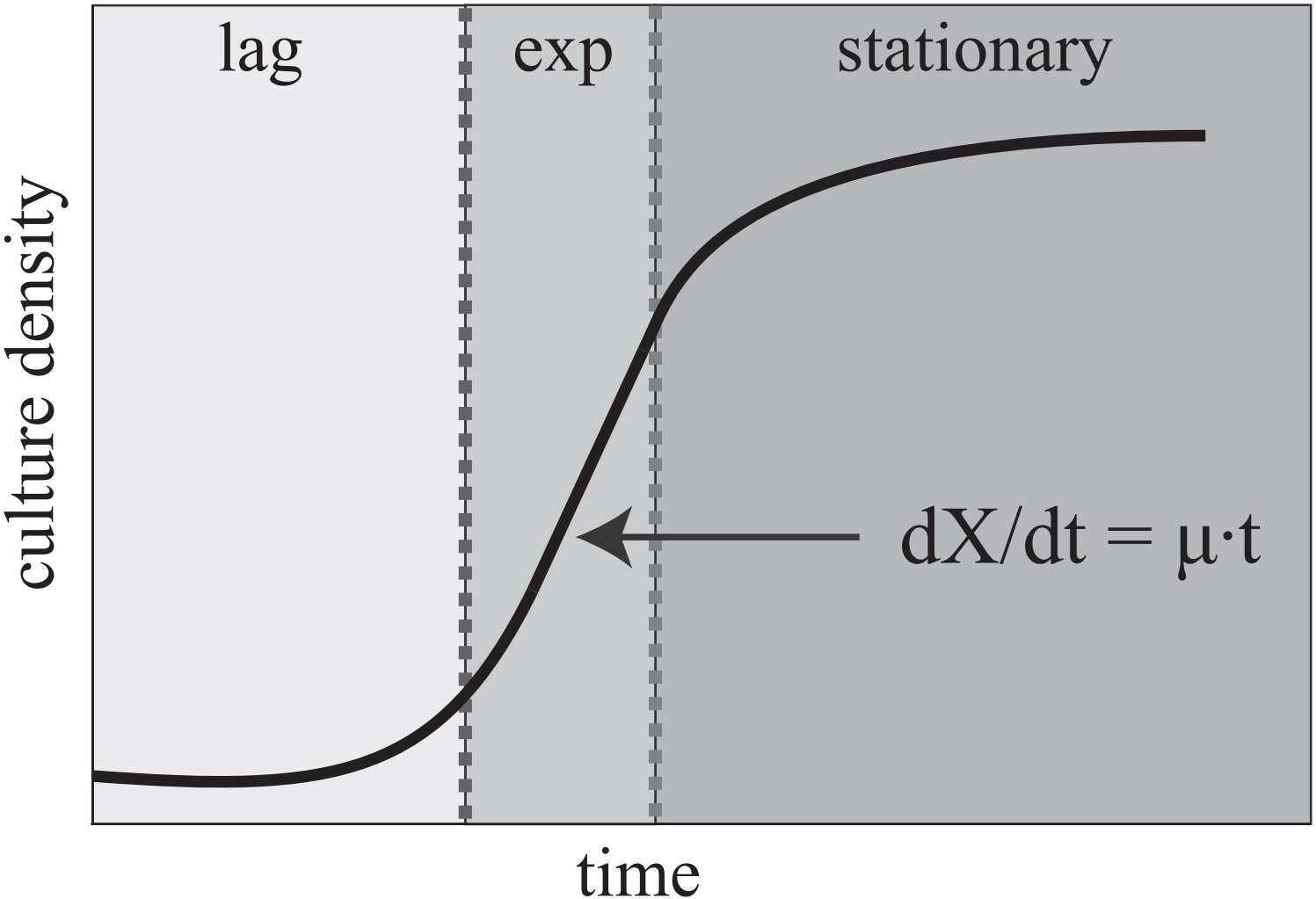
lag
exp
stationary
culture density
dX/dt = μ·t
time

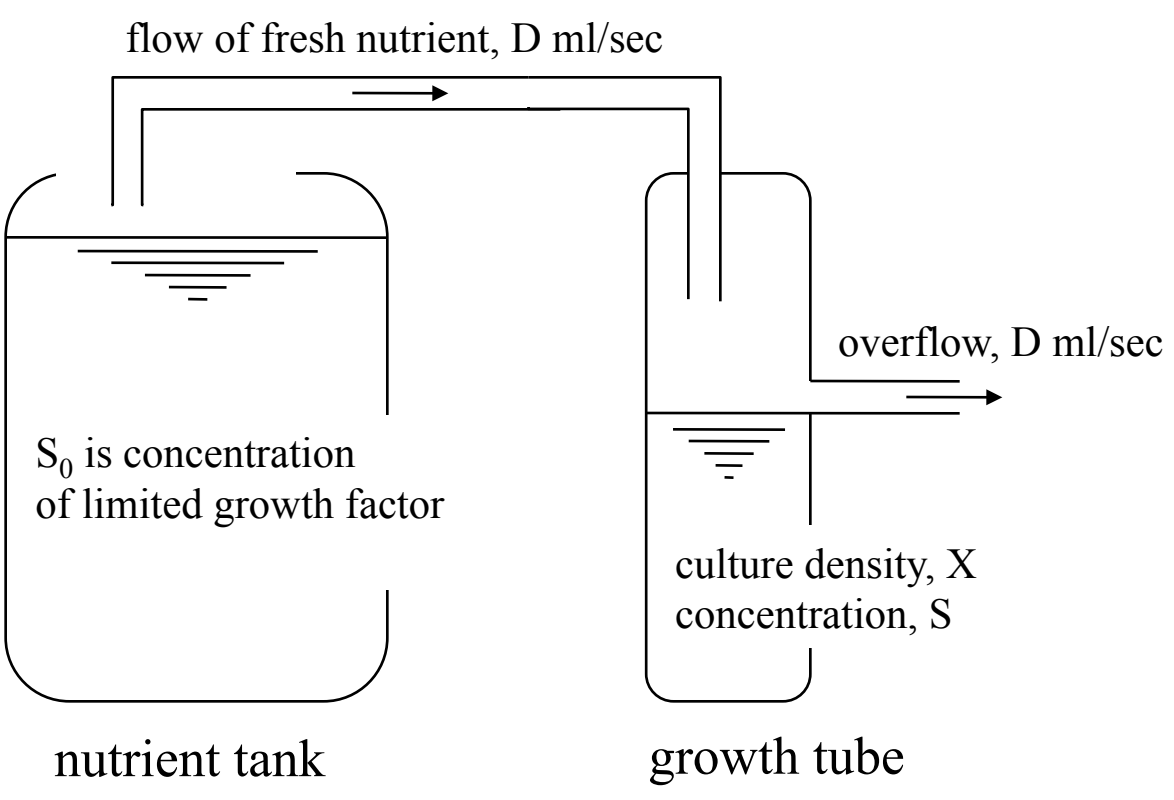
flow of fresh nutrient, D ml/sec
overflow, D ml/sec
$S_0$ is concentration
of limited growth factor
culture density, X
concentration, S
nutrient tank
growth tube

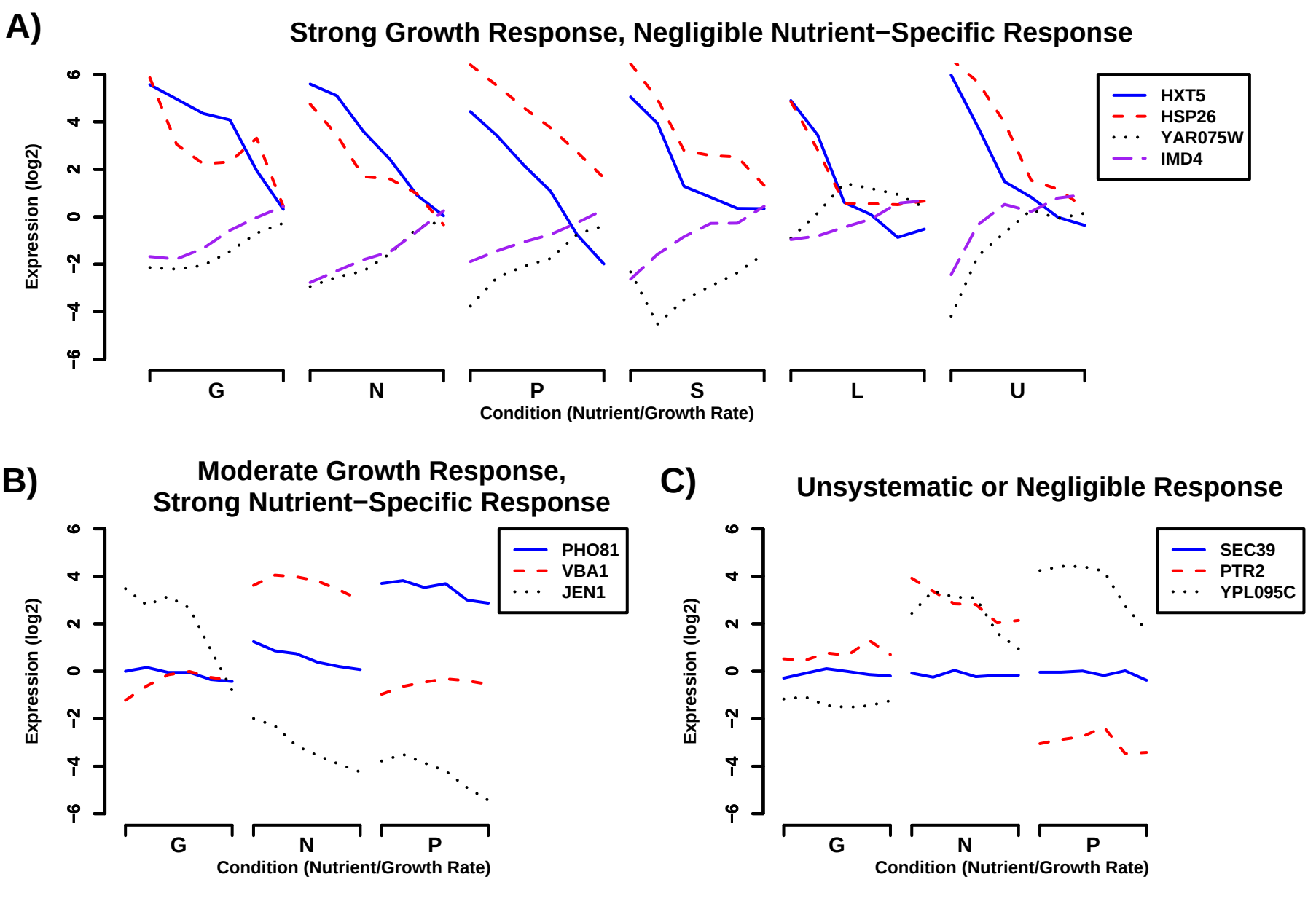
A)
Strong Growth Response, Negligible Nutrient−Specific Response
Expression (log2)
6
4
2
0
−2
−4
−6
HXT5
HSP26
YAR075W
IMD4
G
N
P
S
L
U
Condition (Nutrient/Growth Rate)
B)
Moderate Growth Response,
Strong Nutrient−Specific Response
PHO81
VBA1
JEN1
C)
Unsystematic or Negligible Response
SEC39
PTR2
YPL095C

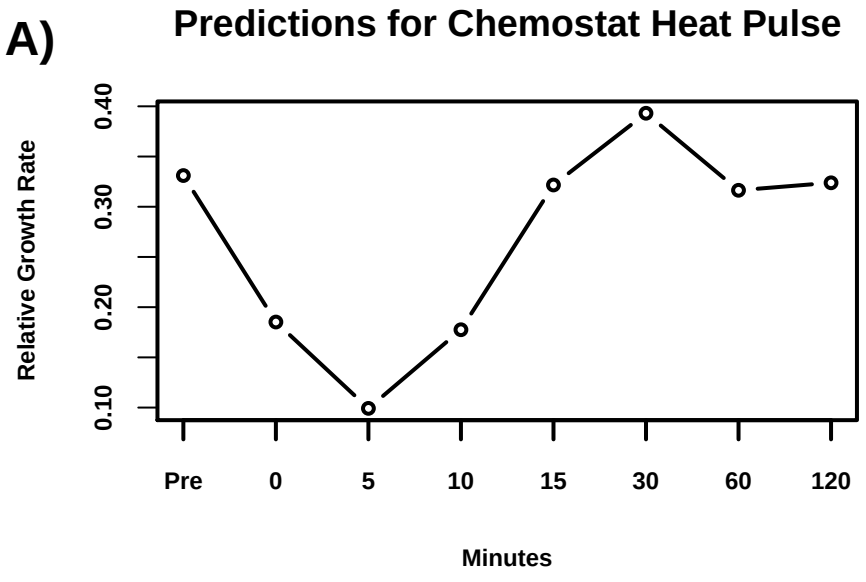
A)
Predictions for Chemostat Heat Pulse
Relative Growth Rate
0.10
0.20
0.30
0.40
Pre
0
5
10
15
30
60
120
Minutes

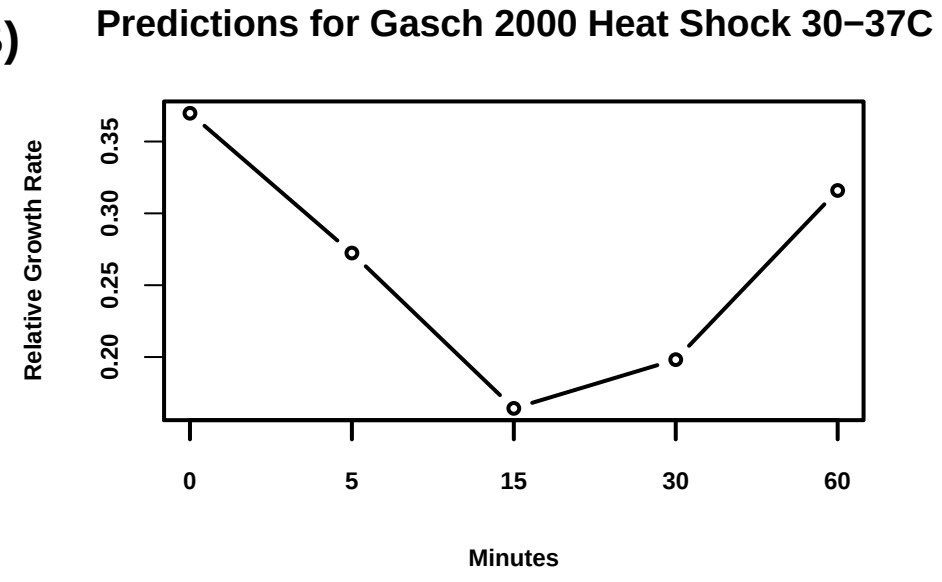
B)
Predictions for Gasch 2000 Heat Shock 30−37C
Relative Growth Rate
0.20
0.25
0.30
0.35
0
5
15
30
60
Minutes

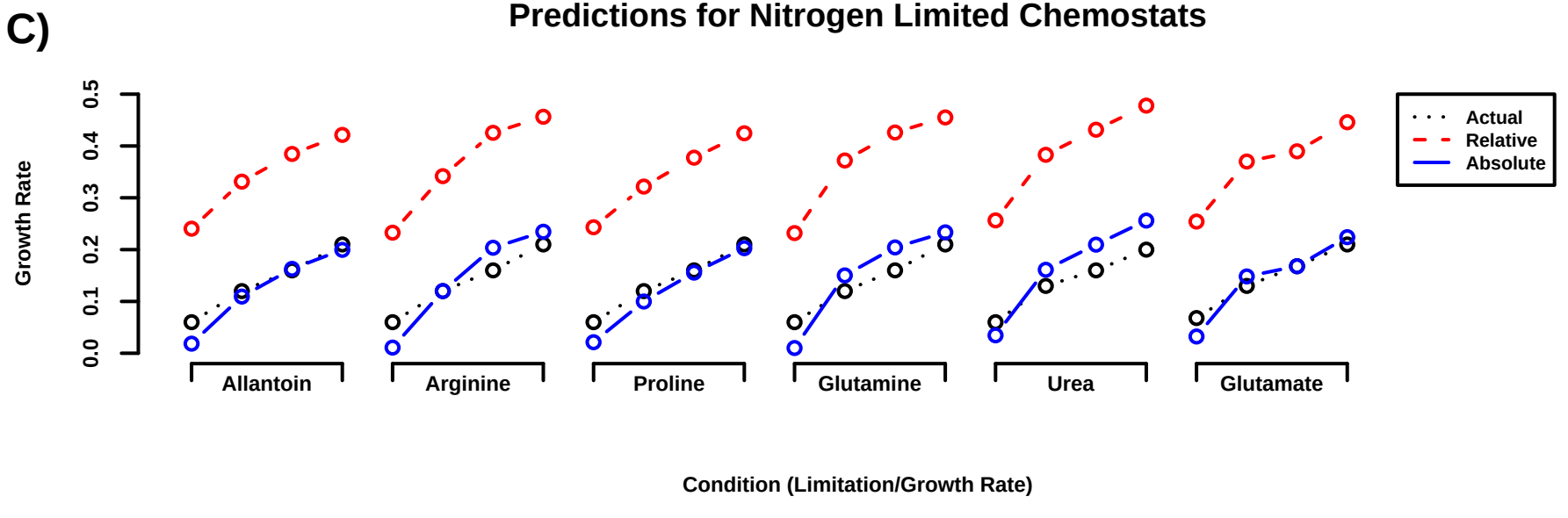
C)
Predictions for Nitrogen Limited Chemostats
Growth Rate
0.0
0.1
0.2
0.3
0.4
0.5
Actual
Relative
Absolute
Allantoin
Arginine
Proline
Glutamine
Urea
Glutamate
Condition (Limitation/Growth Rate)

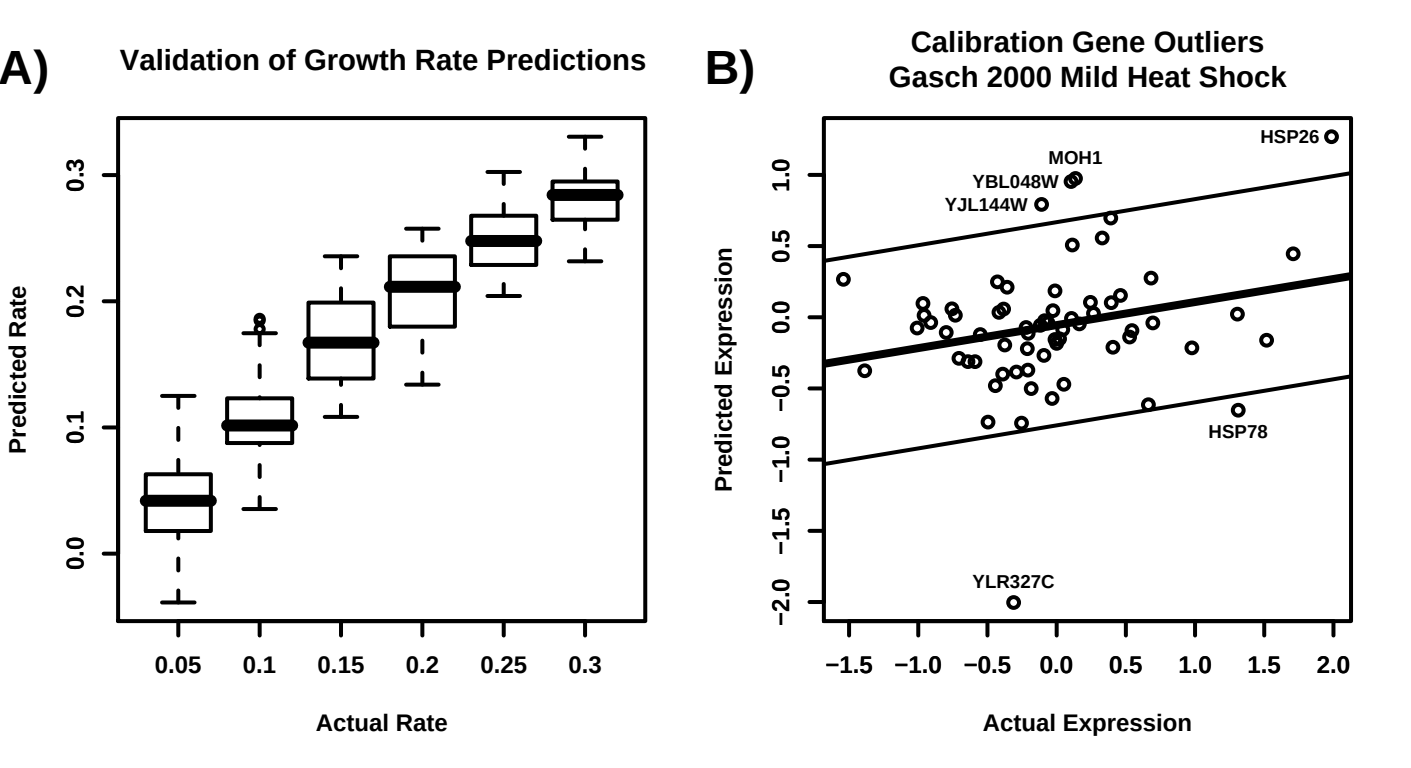
A)
Validation of Growth Rate Predictions
Predicted Rate
0.0
0.1
0.2
0.3
0.05
0.1
0.15
0.2
0.25
0.3
Actual Rate
B)
Calibration Gene Outliers
Gasch 2000 Mild Heat Shock
Predicted Expression
HSP26
MOH1
YBL048W
YJL144W
HSP78
YLR327C
1.0
0.5
0.0
−0.5
−1.0
−1.5
−2.0
−1.5
−1.0
−0.5
0.0
0.5
1.0
1.5
2.0
Actual Expression

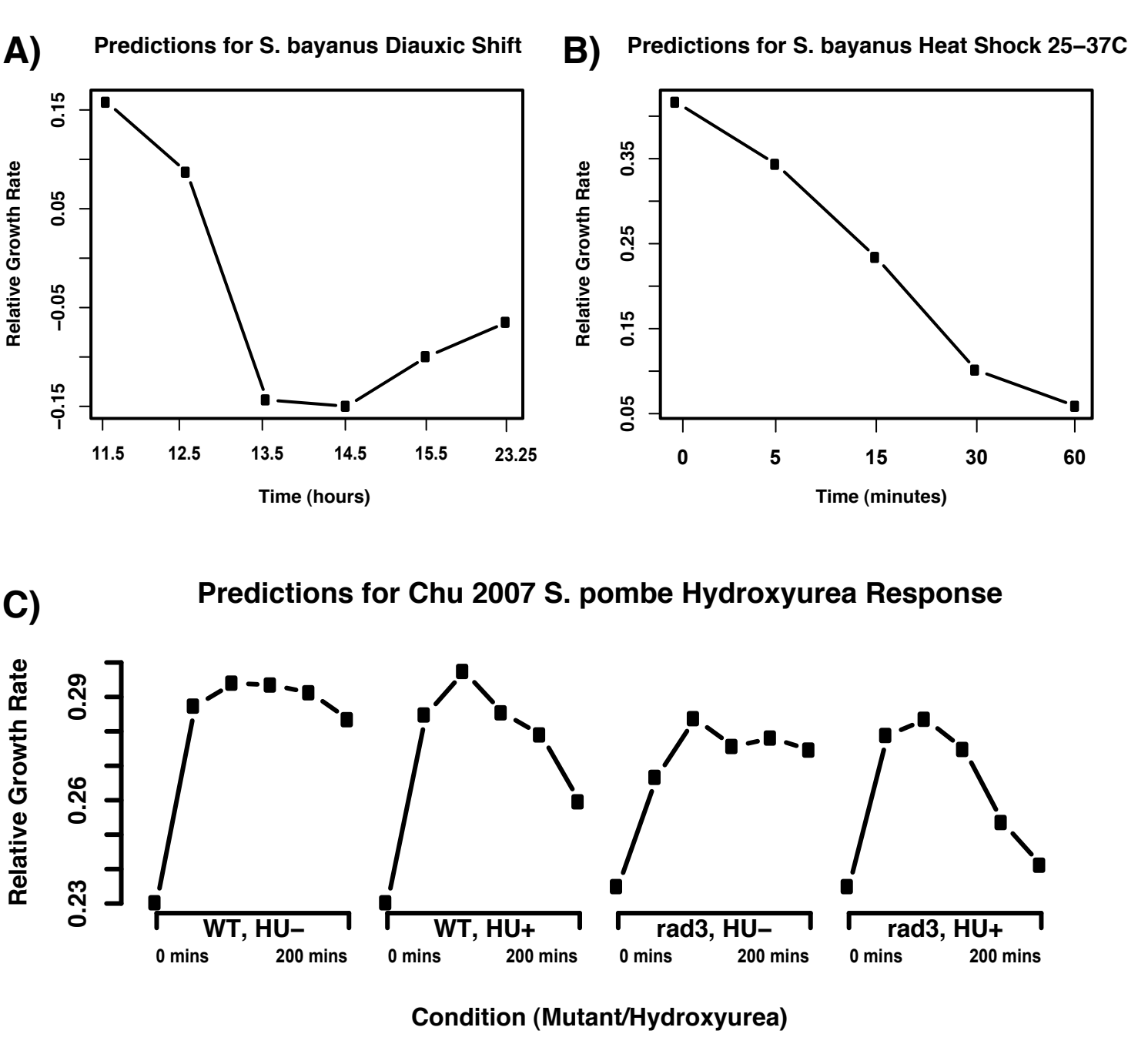
A)
Predictions for S. bayanus Diauxic Shift
Relative Growth Rate
0.15
0.05
−0.05
−0.15
11.5
12.5
13.5
14.5
15.5
23.25
Time (hours)
B)
Predictions for S. bayanus Heat Shock 25–37C
Relative Growth Rate
0.35
0.25
0.15
0.05
0
5
15
30
60
Time (minutes)
C)
Predictions for Chu 2007 S. pombe Hydroxyurea Response
Relative Growth Rate
0.29
0.26
0.23
WT, HU–
WT, HU+
rad3, HU–
rad3, HU+
0 mins
200 mins
Condition (Mutant/Hydroxyurea)

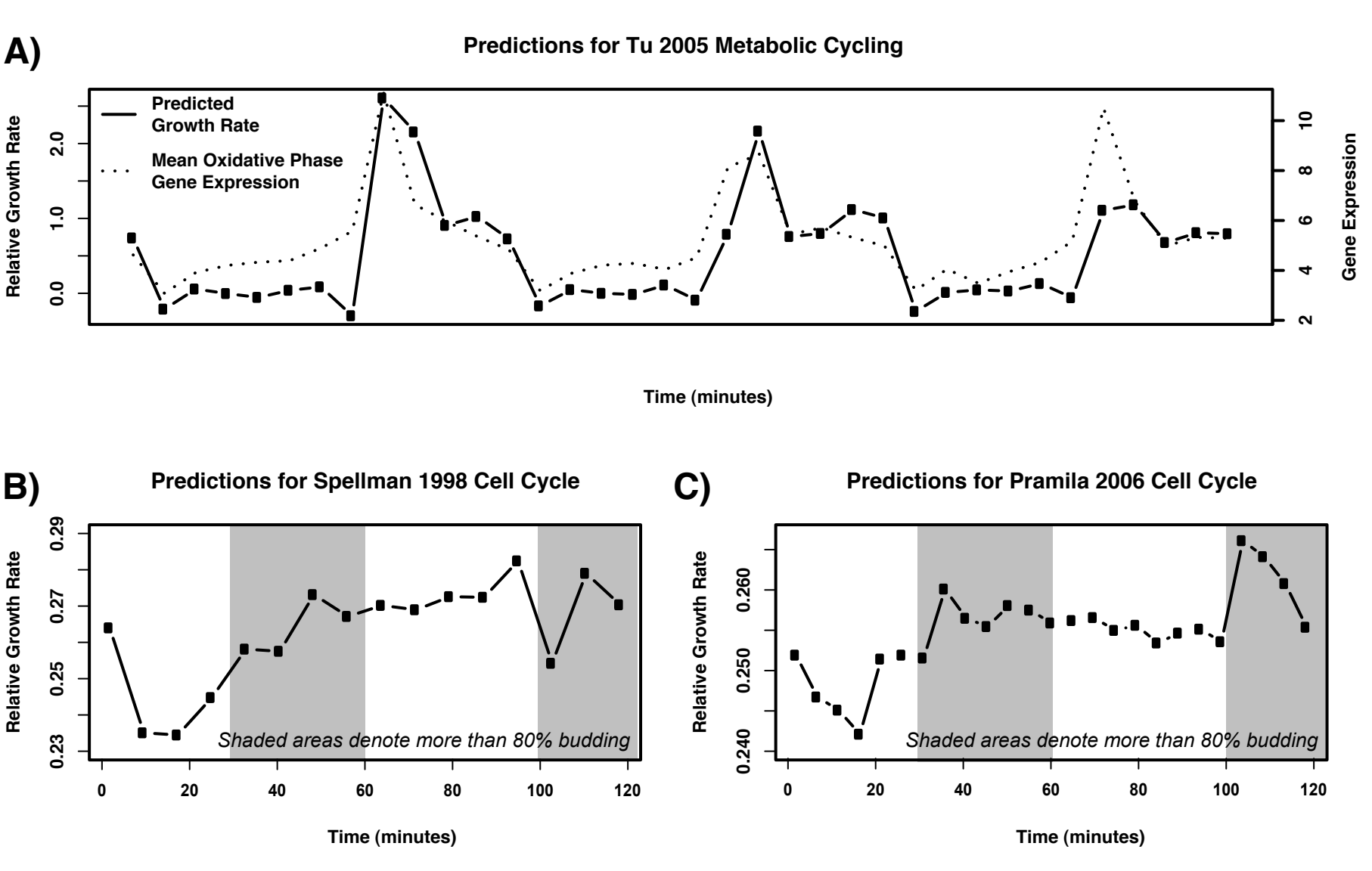
A)
Predictions for Tu 2005 Metabolic Cycling
Predicted
Growth Rate
Mean Oxidative Phase
Gene Expression
Relative Growth Rate
Gene Expression
Time (minutes)
B)
Predictions for Spellman 1998 Cell Cycle
Relative Growth Rate
Shaded areas denote more than 80% budding
Time (minutes)
C)
Predictions for Pramila 2006 Cell Cycle
Relative Growth Rate
Shaded areas denote more than 80% budding
Time (minutes)

A)

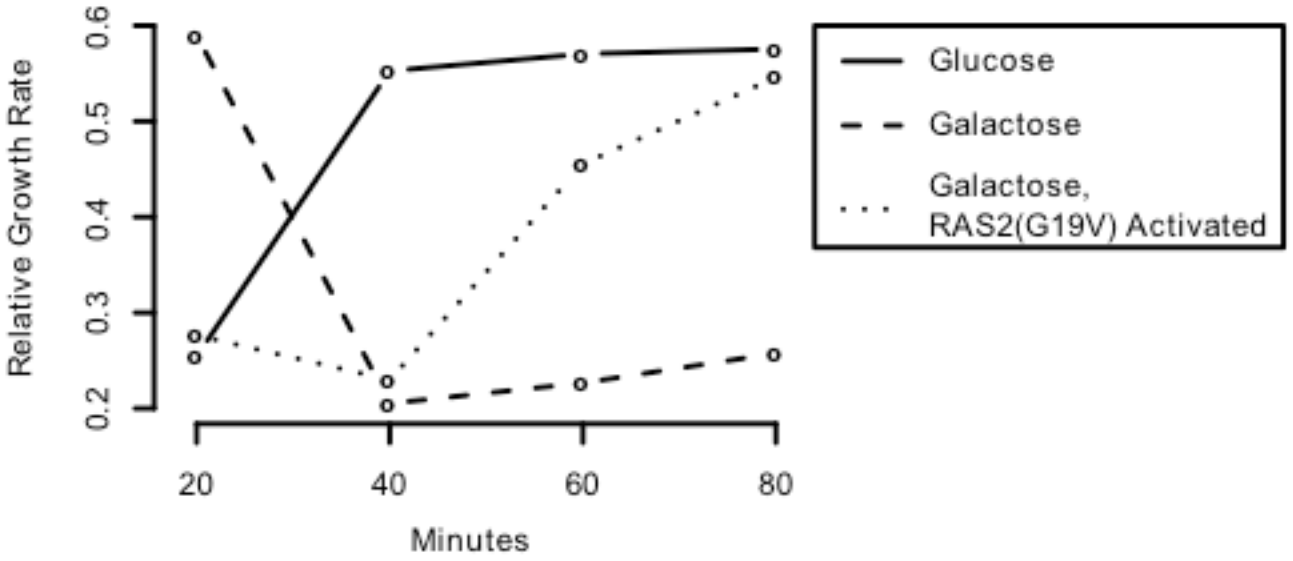
Predictions for Ras/PKA Activation
Relative Growth Rate
0.2
0.3
0.4
0.5
0.6
20
40
60
80
Minutes
Glucose
Galactose
Galactose, RAS2(G19V) Activated

B)

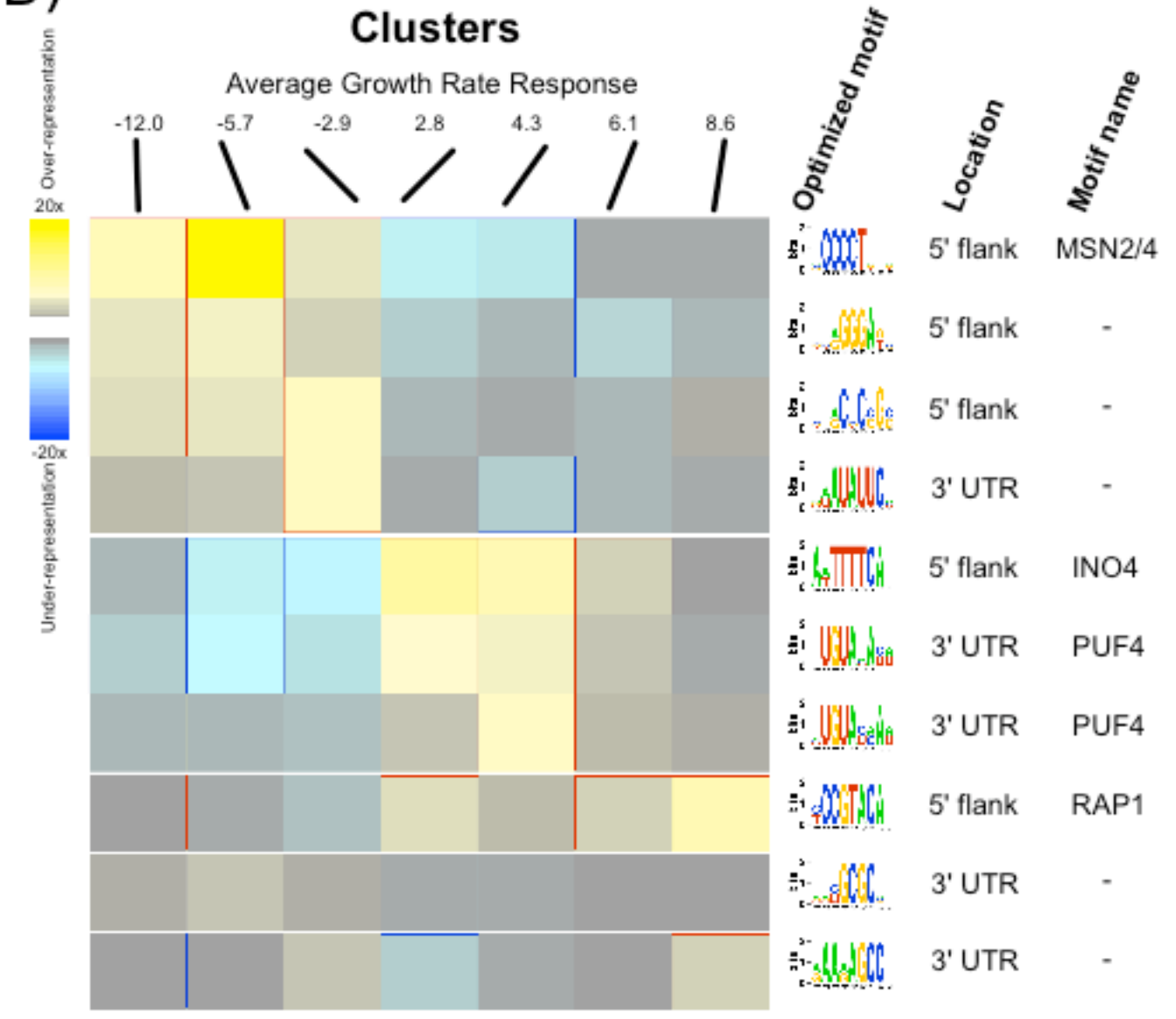
Clusters
Average Growth Rate Response
-12.0
-5.7
-2.9
2.8
4.3
6.1
8.6
Over-representation
20x
-20x
Under-representation
Optimized motif
Location
Motif name
5' flank
MSN2/4
5' flank
-
5' flank
-
3' UTR
-
5' flank
INO4
3' UTR
PUF4
3' UTR
PUF4
5' flank
RAP1
3' UTR
-
3' UTR
-